Divergent Syntheses of Near-Infrared Light Activated Molecular Jackhammers to Eradicate Cancer Cells

Bowen Li,[1] Ciceron Ayala-Orozco,[1]* Tengda Si,[1] Lixin Zhou,[1] Zicheng Wang,[1] Angel A. Martí,[1,2,3] James M. Tour[1,2,3,4]*

[1]Department of Chemistry, Rice University, Houston, Texas 77005, USA.

[2]Smalley-Curl Institute, Rice University, Houston, Texas 77005, USA.

[3]Department of Materials Science and Nanoengineering, Rice University, Houston, Texas 77005, USA.

[4]NanoCarbon Center and the Rice Advanced Materials Institute, Rice University, Houston, Texas 77005, USA.

*Corresponding author: ca5@rice.edu; tour@rice.edu

Abstract Aminocyanines involving Cy7 and Cy7.5 amines function as molecular jackhammers (MJH) by vibronic-driven action (VDA). That has been demonstrated through the coupling of the molecular vibrational and electronic modes, causing picosecond whole-molecule concerted stretching. If the molecules are cell-associated and then activated by near infrared light, the VDA mechanically disrupts the cell membranes resulting in the rapid death by necrosis. Distinct from photodynamic therapy and photothermal therapy, VDA with its ultrafast vibrational action is not slowed by high concentrations of reactive oxygen species (ROS) scavengers. With the importance of these MJH libraries, their efficient syntheses are here disclosed. We report a practical approach

to access the key intermediate, facilitating the preparation of various Cy7 and Cy7.5 MJH in moderate and high yields with diverse side chains to study structure-activity relationships.

Keywords aminocyanines, molecular jackhammers, vibronic-driven action, structure-activity relationships

Introduction

Globally, cancer stands as a life-threatening malignant disease involving more than 100 different types and ranking as the second leading cause of death.[1-4] At present, phototherapy has gained recognition as a minimally invasive treatment for cancer, providing improved tissue specificity[5-8] and remarkably reduced side effects in comparison with traditional cancer therapies.[9-11] Phototherapy includes two categories: photodynamic therapy (PDT)[12-18] and photothermal therapy (PPT),[19-22] where photosensitizers play a pivotal role in converting light energy into either reactive oxygen species (ROS) or heat, thereby inducing cancer cell death.[23-25] Furthermore, synergistic strategies that combine PDT and PTT is being studied because the treatment efficiency of PDT or PTT alone typically decreased under hypoxic or heat shock environments.[26-28] Despite the significant progress achieved in both PDT and PTT, it is necessary to develop more effective light-based strategies to enhance cancer treatments.

We have developed a concept called vibronic-driven action (VDA) with Cy7.5 amine,[34] a mechanical action that incorporates coupling of a molecule's vibrational with its electronic

mode,[29,30] in the form of a molecular plasmon,[31-33] that induces longitudinal and axial stretching of the molecules. These stretching modes are whole-molecule-based and termed molecular jackhammers (MJH).[34] This concept has demonstrated significant efficiency in eradicating human melanoma cells by mechanically disassembling membranes with MJH through VDA. These light-activated mechanical actions are clearly distinguishable from PDT and PTT (Figure 1a).[34,35] The VDA mechanical effect on the cell membrane is not retarded by high doses of inhibitors of ROS, and VDA does not induce an increase in the temperature of the media.[34]

Cyanine dyes feature two nitrogen-containing heterocycles, wherein one carries a positive charge and is conjugated through a polymethine bridge to the other nitrogen center.[38-41] These dyes exhibit distinctive properties, such as high molar extinction coefficients with narrow absorption bands. The core structure of Cy 7 and Cy 7.5 amines are shown in Figure 1b and they incorporate cyclohexene rings in the polymethine bridge, enhancing the structure rigidity and improving stability, thereby increasing photostability and quantum yield.

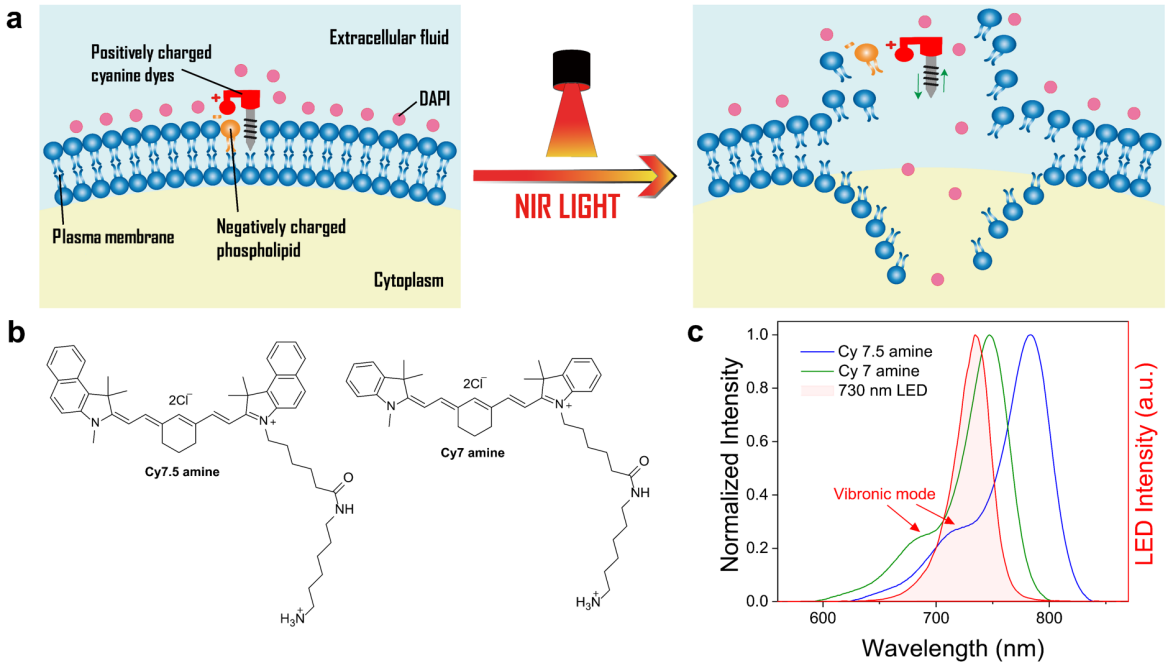

Figure 1. The model of molecular jackhammer to open cell membranes, chemical structures, and UV-vis spectrum. A) Proposed mechanisms of MJH opening cell membranes. B) Chemical structures of Cy 7 amine, Cy 7.5 amine and their core structure. C) Absorption spectra of Cy 7 and Cy7.5 amines, along with the assignment of vibrational collective oscillation (vibronic mode).

The absorption spectrum of Cy 7 and Cy 7.5 amines (Figure 1c) is featured by a sharp and intense absorption band in the near-infrared (NIR), and with an additional vibronic shoulder located at higher energies at lower wavelengths.[34,37] In our previous work, we combined experimental results with theoretical calculations, and observed a vibronic mode at 680 nm for Cy 7 amine and 730 nm for Cy7.5 amine. This observation supports the assumption that Cy7.5 amine (excitation at 730 nm) was more efficient than Cy 7 amine (excitation at 680 nm) in opening A375 cell membranes due to the higher plasmonicity of the benzoindole as compared to indole.[34,35]

Despite the recent progress in biomedical applications of Cy 7 and Cy 7.5 amines, practical and systematic construction of these molecules remains difficult.[42-44] We surmised that the synthesis of the corresponding cyclic glutacondianil immediate **2a** (as indicated in Table 1) and its subsequent substitution would provide a straightforward approach to these compounds. However, achieving this was challenging due to the instability of **2a**. Recent work from Burgess and co-workers successfully accomplished the synthesis of **2a** through a Vilsmeier–Haack reaction starting from cyclohexene, but with harsher conditions resulting in depressed yields.[42] In this work, we present a synthetic approach for obtaining various Cy7 and 7.5 MJH that incorporate diverse substituents on their heterocyclic groups. These analogues were successfully applied with high efficiency to eradicate several cancer cell lines through VDA under NIR light irradiation.

Table 1. Optimization for the synthesis of key intermediate 2 from salt 1.

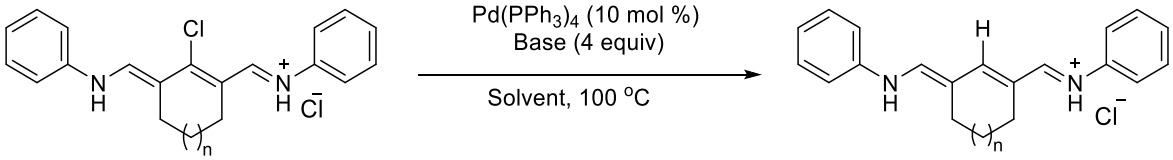

n = 1, **1a**
n = 0, **1b**

n = 1, **2a**
n = 0, **2b**

Entry[a]	N	Base	Solvent	Yield (%)[b]
1	1	K_3PO_4	DMF/H_2O (5:1)	31
2	1	K_2HPO_4	DMF/H_2O (5:1)	30
3	1	KF	DMF/H_2O (5:1)	25
4	1	K_2CO_3	DMF/H_2O (5:1)	32
5	1	NaO*t*Bu	DMF/H_2O (5:1)	0

Entry[a]	N	Base	Solvent	Yield (%)[b]
6	1	NaOAc	DMF/H_2O (5:1)	0
7	1	CsF	DMF/H_2O (5:1)	3
8	1	Cs_2CO_3	DMF/H_2O (5:1)	10
9	1	K_2CO_3	DMF/H_2O/IPA (5:1:1)	35
10	1	K_2CO_3	EtOH	37
11	1	K_2CO_3	IPA	66 (61)[c]
12[d]	1	K_2CO_3	IPA	77
13[e]	1	K_2CO_3	IPA	68
14[f]	0	K_2CO_3	IPA	75
15	2	K_2CO_3	IPA	trace

[a] The reactions were carried out with conditions: 1) **1** (0.25 mmol, 1 equiv), $Pd(PPh_3)_4$ (10 mol %), base (4 equiv) in solvent at 100 °C for 24 h; [b] yields were determined by HPLC on a C18 reverse-phase column; [c] isolated yield; [d] 48 h, isolated yield; [e] **1a** (8.38 mmol), 48 h, isolated yield; [f] **1b** (2.91 mmol), 48 h, isolated yield.

Results and discussion

We began our investigation of dehalogenation reaction by using Schiff base **1a**[46] as a model substate (Table 1). Encouragingly, we observed the formation of product **2a** from these substrates, achieving 31% yield under the condition of 10 mol % of $Pd(PPh_3)_4$ as catalyst, DMF/H_2O as solvent. Preliminarily, we systematically assessed various bases (entries 1-8) and found that K_2CO_3 provided a superior yield, while the use of stronger base (entry 5) or weaker base (entry 6) failed to provide the desired product **2a**. Further investigation using various solvents (entries 9-11)

indicated isopropyl alcohol (IPA), possessing a β-hydrogen as the likely hydrogen source, was highly effective in promoting the dechlorination reaction, providing product **2a** in 66% yield (61% isolated yield, entry 11). By extending the reaction time from 24 h to 48 h, the yield can be increased to 77% as in entry 12. This strategy demonstrated scalability, affording multigram-scale product **2a** with 68% yield (entry 13). Likewise, the same protocol was successful in five-membered product **2b** with good yield (entry 14).[45] However, application of the reaction scheme to the seven-membered substrate resulted in only trace amounts of product (entry 15), presumably due to its twisted conformation.

Having established the key intermediate **2**, we investigated the scope of substitutions, which are detailed in Table 2.[47-50] The symmetrical analogues ranging from **4a** to **4o** were synthesized by one step between **2** and heterocyclic salts **3** in the presence of NaOAc at 80 °C in EtOH, all in satisfactory yields. Various functional substituents, such as methyl (**4a)**, carboxylic acid (**4i)**, ester (**4j**), dimethylaminos (**4h** and **4k**), 1,3-dioxoisoindolin-2-yl (**4l**) and dimethylcarbamoyl (**4g**) were well tolerated, forming the corresponding products in moderate to good yields (54-84%). Subsequently, we assessed the reactivity associated with identical substitution of side chains bearing different heterocyclics. A benzoindolium salt produced product **4b** in 79% yield. **4c** and **4d** were formed from quinolinium and indolium-based heterocycles, respectively, both accomplished in good yields (70% and 83%). The pyrrolidine-based heterocycle was also applicable with the current protocol (**4e**), providing the desired product in 50% yield.

Table 2. Synthesis of the Cy7/Cy7.5 amine analogues 4 from *N*-heterocyclic salt 3/3' and key intermediate 2.[a]

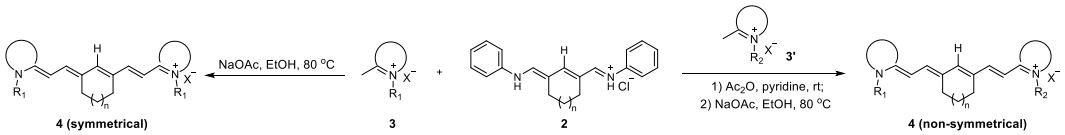

4 (symmetrical) **3** **2** **4 (non-symmetrical)**

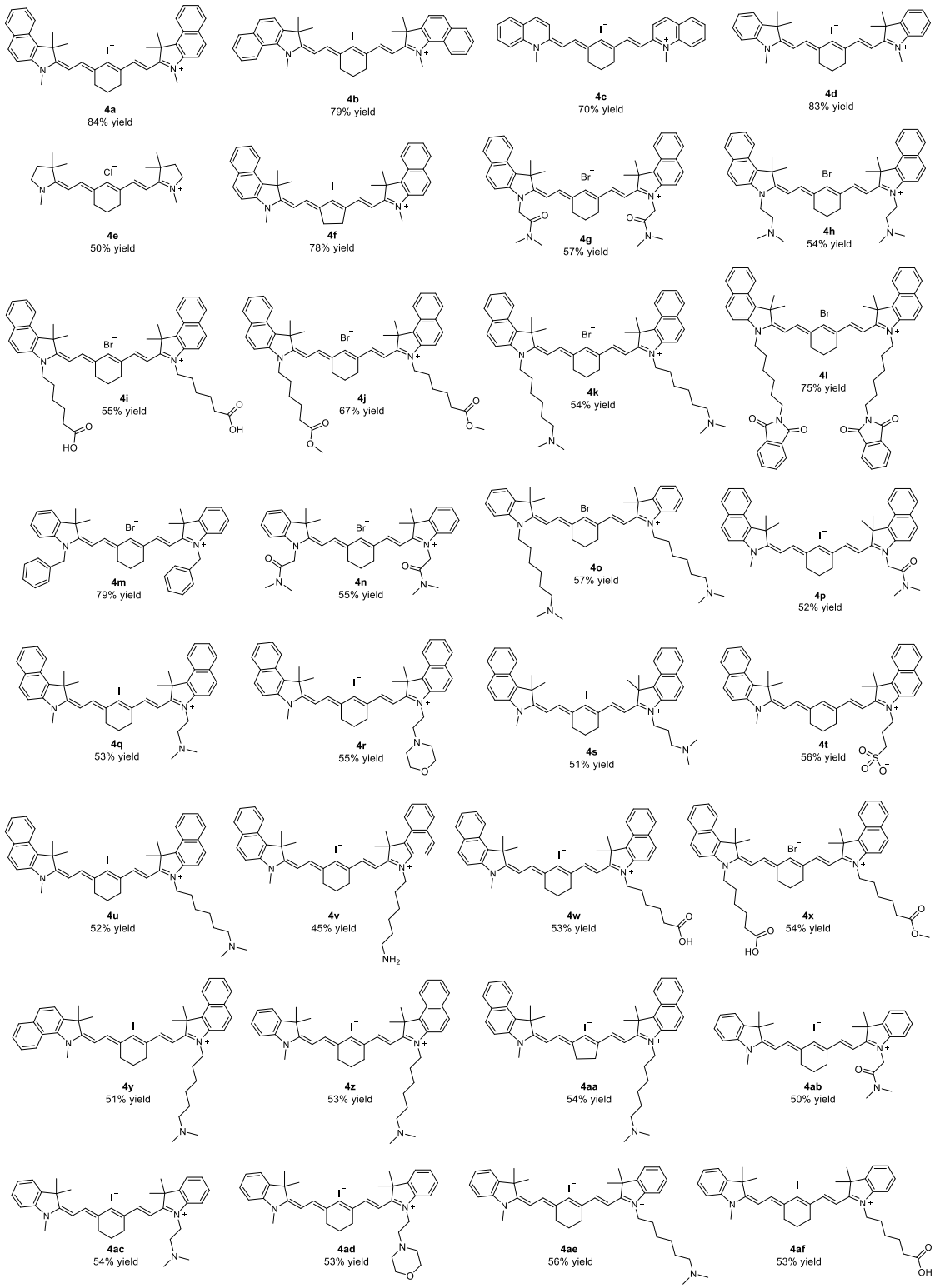

[a] Reaction conditions for synthesis of symmetrical **4** (**4a**-**4o**): **3** (2.0 equiv), **2** (1.0 equiv), and NaOAc (3.0 equiv) in EtOH at 80 °C; nonsymmetrical **4** (**4p**-**4af**): 1) **3** (1.0 equiv), **2** (1.0 equiv) in Ac_2O and pyridine at rt; 2) **3'** (1.0 equiv), and NaOAc (3.0 equiv) in EtOH at 80 °C; isolated yields.

The synthesis of nonsymmetric analogues from **4p** to **4af** took two steps: first, reaction of equimolar amounts of **2** and heterocyclic salts **3** in Ac_2O and pyridine. The corresponding acetylated precursors were condensed with equimolar amounts of heterocycles with various substitutions **3'**.[51-53] Likewise, products featuring several *N*-alkyl substitutions, including dimethylcarbamoyl (**4p**), dimethylamino (**4q**, **4s** and **4u**), morpholino (**4r**), and sulfonate (**4t**), were obtained by conducting the condensation sequence, albeit in moderate yields (51-56%) mainly owing to the inevitable formation of the competing symmetrical byproducts. The substrate with an aminohexyl substituent delivered **4v** in inferior yield (45%). In addition, employing identical *N*-alkyl substitutions for both indolium-based salts (**4ab**-**4af**) and benzoindoles, led to similar yields. Products featuring distinct heterocyclics, specifically **4y** from a benzoindolium salt with different positions and **4z** from an indolium salt, were achieved with yields of 51% and 53%, respectively. Analogues containing five-membered rings **4f** and **4aa**, were also synthesized with yields of 78% and 54%, respectively, comparable to those of six-membered rings.

Photophysical Characterization

The photophysical properties, including absorption (λ_{abs}) maxima, emission (λ_{em}) maxima, molar extinction coefficients (ε) and quantum yields (Φ_F), for all molecules were determined in methanol (Figure S1-S34 of Supporting Information), and the summarized data are presented in Table 3.[37,43] The absorption spectra exhibit one major absorption band with maxima in the range of 744-748 nm, characteristic of Cy 7 dyes, and 780-788 nm for Cy7.5 dyes. Similar features are displayed in the emission spectra, with maxima at 766-773 nm for Cy 7 dyes and 802-816 nm for Cy7.5 dyes. Small stokes shifts, ranging from 15-26 cm^{-1}, were observed.

Table 3. Photophysical Properties of the Prepared Cyanine Dyes in Methanol.

Cyanine dyes	λ_{max}(abs)/nm	λ_{max}(em)/nm	$\Delta\lambda$/nm	ε_{max}[a]	Φ_F
ICG	784	812	28	2.33×10^5	0.063
4a	780	801	21	2.55×10^5	0.074
4b	791	816	25	2.82×10^5	0.027
4c	789	815	26	1.61×10^5	0.037
4d	744	765	21	2.04×10^5	0.130
4e	648	668	20	0.80×10^5	0.052
4f	818	837	19	2.02×10^5	0.037
4g	780	804	24	3.24×10^5	0.077
4h	785	809	24	2.41×10^5	0.074
4i	787	808	21	3.12×10^5	0.089
4j	785	808	23	2.29×10^5	0.072
4k	788	809	21	2.39×10^5	0.078

Cyanine dyes	λ_{max}(abs)/nm	λ_{max}(em)/nm	$\Delta\lambda$/nm	ε_{max}[a]	Φ_F
4l	788	808	20	2.35×10^5	0.091
4m	752	773	21	2.63×10^5	0.130
4n	745	767	22	3.26×10^5	0.125
4o	751	772	21	2.03×10^5	0.123
4p	780	802	22	2.49×10^5	0.063
4q	782	806	24	2.33×10^5	0.073
4r	781	807	26	2.82×10^5	0.077
4s	783	804	21	2.35×10^5	0.066
4t	783	804	21	2.17×10^5	0.064
4u	785	804	19	2.43×10^5	0.065
4v	784	804	20	2.02×10^5	0.061
4w	783	804	21	2.69×10^5	0.075
4x	787	808	21	2.84×10^5	0.085
4y	787	812	25	2.26×10^5	0.033
4z	765	787	22	2.95×10^5	0.079
4aa	823	838	15	2.20×10^5	0.040
4ab	744	766	22	2.62×10^5	0.125
4ac	746	768	22	2.54×10^5	0.111
4ad	748	769	21	2.81×10^5	0.117
4ae	747	768	21	2.38×10^5	0.129
4af	748	769	21	2.58×10^5	0.139

[a]All values were determined using 1 μM cyanine dye solutions at 25 °C. ε_{max}/mol^{-1} L cm^{-1}. Quantum yields were determined using ICG (Φ_F = 0.13 in DMSO) as standard.

In general, the presence of side chains in these compounds did not significantly affect the maximum absorption wavelength or the curve shapes, except for notable changes in molar extinction coefficients (for **4g**, **4i**, reaching up to ~3 × 10^5 $M^{-1}cm^{-1}$). The substitution of side chains bearing different heterocyclic dyes were observed to have a significant influence on the absorption maxima, while the Stokes shifts appeared to be relatively insensitive to the different side chains. Nonsymmetric dye **4z** derived from indolium and benzoindolium salts, exhibiting a maximum absorption wavelength between Cy 7 and Cy 7.5 dyes, specifically at 765 nm. Cyclopentene rings in **4f** and **4aa** induced a bathochromic shift of the maximum to 818 nm and 823 nm, respectively, compared to the cyclohexene rings **4a** and **4u**. Conversely, the presence of the pyrrolidine salts in **4e** resulted in a blue shift of the maximum to 648 nm. Moreover, most synthesized dyes showed higher fluorescence quantum yields than indocyanine green (ICG).[54] ICG is the only FDA-approved NIR fluorescent cyanine dye, possessing commercially available, non-toxic, relatively stable, amphiphilic properties and its quantum yield in DMSO has been characterized.[37,54] Notably, the brightness of **4af** exhibited a 2.2-fold improvement over ICG. The use of cyclopentene rings instead of cyclohexene rings **4f** and **4aa**, pyrrolidine **4e** and quinoline salts **4c**, decreases the quantum yields.

Assessment of VDA activity of MJH for permeabilization of cell membranes

Flow cytometry analysis was conducted to evaluate the VDA activity of MJH on permeabilizing the cellular membrane on KPC pancreatic cancer cells[55-58] under NIR light activation (730 nm, 80 mW/cm^2 for 10 min) *in vitro* (Figure 2 and Figure S35-S37). KPC has *LSL-Kras$^{G12D/+}$, LSL-Trp53$^{R172H/+}$,* and *Pdx-1-Cre* mutations, an established and most extensively preclinically studied genetic model of pancreatic ductal adenocarcinoma (PDAC), exhibiting numerous significant features observed in human PDAC.[56,58] Here the VDA activity of MJH is compared against the controls without light activation. In this assessment, MJH molecules with benzoindole (strong MJH: **4q** and **4u**) versus indole (weak MJH: **4ac** and **4ae**) are compared.[34] When the cell membranes are ruptured, a blue-fluorescent dye 4′,6-diamidino-2-phenylindole (DAPI) enters the cell and immediately stains the nucleus. This is indicative of a rapid necrotic cell death and DAPI cell membrane permeabilization by the MJH exhibiting VDA. The effective concentration needed to permeabilize 50% of the cells (VDA IC_{50}) was estimated for each molecule (Figure S37). Consistently, we observed that MJH containing benzoindole are more effective to permeabilize KPC cancer cells.[34] In addition, we show that ROS scavengers are not able to inhibit the VDA mediated by light-activated MJH (Figure 2k-l). This suggest that the VDA is different than PDT.[59] We validated the effectiveness of ROS scavenger mixture (100 mM thiourea and 2.5 mM sodium azide) to stop ROS-mediated cell membrane permeabilization.[36] We showed that exposure of the KPC cells to 50 mM H_2O_2 for 1 h effectively permeabilizes the cells (Figure 2-k11 and 2-l11). However, the ROS scavenger mixture (100 mM thiourea and 2.5 mM

sodium azide) is highly effective in preventing the cell membrane permeabilization by ROS (Figure 2-k12 and 2-l12). Overall, with these controls, the data continues to support the supposition that VDA works differently than PDT.[59]

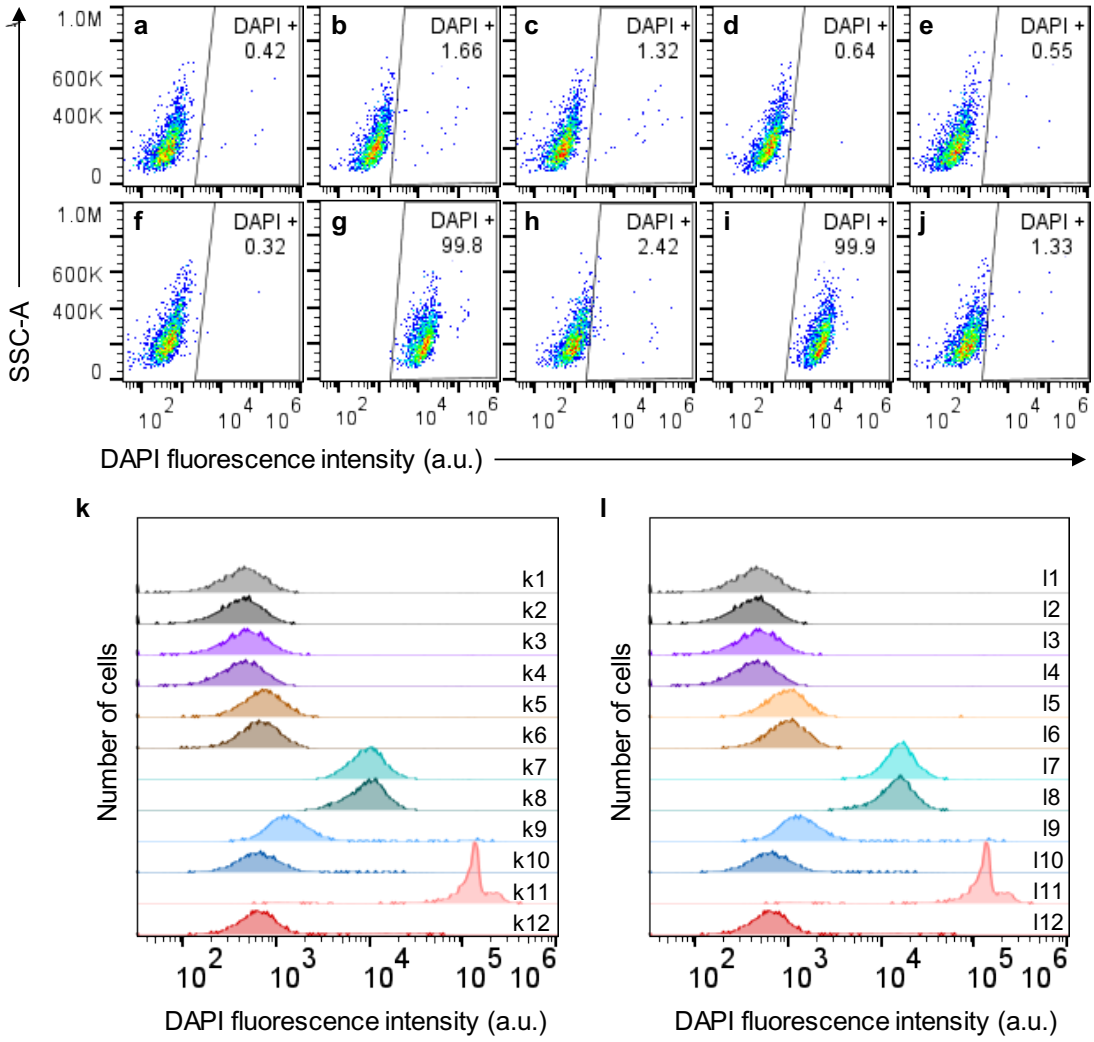

Figure 2. Assessment of MJH-mediated cell membrane permeabilization thought flow cytometry analysis in KPC cells. Molecules with benzoindole (**4q** and **4u**) versus indole (**4ac** and **4ae**) are compared. a-b) Flow cytometry analysis of cell suspension samples without light activation: a) 0.1% DMSO, b) 0.5 µM **4q**, c) 0.5 µM **4ac**, d) 0.5 µM **4u** and e) 0.5 µM **4ae**. f-j)

Flow cytometry analysis of cell suspension samples treated with light activation: f) 0.1% DMSO + NIR light, g) 0.5 μM **4q** + NIR light, h) 0.5 μM **4ac** + NIR light, i) 0.5 μM **4u** + NIR light and j) 0.5 μM **4ae** + NIR light. k-l) Assessment of ROS contributions through addition of ROS inhibitors (100 mM thiourea and 2.5 mM sodium azide) and/or hydrogen peroxide (H_2O_2, 50 mM). k) case of 0.5 μM **4q** and l) case of 0.5 μM **4u**. k1) 0.1% DMSO, k2) 0.1% DMSO + ROS inhibitors, k3) 0.1% DMSO + NIR light, k4) 0.1% DMSO + ROS inhibitors + NIR light, k5) 0.5 μM **4q**, k6) 0.5 μM **4q** + ROS inhibitors, k7) 0.5 μM **4q** + NIR light, k8) 0.5 μM **4q** + ROS inhibitors + NIR light, k9) 50 mM H_2O_2 for 10 min, k10) 50 mM H_2O_2 for 10 min + ROS inhibitors, k11) 50 mM H_2O_2 for 1 h, k12) 50 mM H_2O_2 for 1 h + ROS inhibitors. l1) 0.1% DMSO, l2) 0.1% DMSO + ROS inhibitors, l3) 0.1% DMSO + NIR light, l4) 0.1% DMSO + ROS inhibitors + NIR light, l5) 0.5 μM **4u**, l6) 0.5 μM **4u** + ROS inhibitors, l7) 0.5 μM **4u** + NIR light, l8) 0.5 μM **4u** + ROS inhibitors + NIR light, l9) 50 mM H_2O_2 for 10 min, l10) 50 mM H_2O_2 for 10 min + ROS inhibitors, l11) 50 mM H_2O_2 for 1 h, l12) 50 mM H_2O_2 for 1 h + ROS inhibitors.

Anticancer efficiency of plasmon-driven MJH

To evaluate the anticancer efficiency of MJH in eradicating cancer cell lines under NIR light activation (730 nm, 80 mW/cm^2 for 10 min) *in vitro*, the clonogenic assay[60] was subsequently applied to kill the KPC cells[55-58] under both light and without light conditions following treatment with diverse MJH at various concentrations (Figure 3) and the experimental set up is depicted in Figure 3a. Having demonstrated the highest VDA activity in MJH molecules with benzoindolium

over indolium in permeabilizing cells through flow cytometry analysis, we focus in the subsequent clonogenic assays exclusively on benzoindolium-based MJH. VDA IC_{50}, representing the effective concentration molecules needed to kill 50% of the cell population under light activation and cytotoxicity IC_{50}, representing the inhibitory concentration of molecules needed to inhibit the cell growth by 50% under dark condition. We analyzed twelve MJH, and these results highlight that nonsymmetric molecules exhibit higher activity under light conditions but also demonstrate higher dark toxicity compared to symmetric (Figure 3d and e). The MJH **4p** with dimethylcarbamoyl substitution exhibited the highest VDA activity in contrast to the other molecules (Figure 3b and c, VDA IC_{50} = 74 nM). **4q** and **4h** with dimethylamino ethyl substitutions also demonstrated excellent VDA activity in cancer cell eradication. However, **4h** exhibited significantly lower toxicity than **4q**, possessing the highest phototherapy index (ratio of cytotoxicity IC_{50}/VDA IC_{50}, as shown in Figure 3f) compared to others. Furthermore, **4r** (morpholino) showed comparable activity with **4h** but was more toxic. MJH with amino (Cy 7.5 amine and **4v**), carboxylic acid (**4w**) substitutions indicate relatively lower VDA activities and phototherapy index despite presenting lower toxicity among them. Interestingly, **4aa** with cyclopentene ring substitutions exhibited a notable decrease in VDA activity when compared to **4u**, despite both having similar cytotoxicity IC_{50} values, providing the lowest therapeutic index. Notably, compound **4t**, featuring a sulfonate substitution like ICG,[54] is a comparatively safe MJH, with more than 90% of cells maintaining viability even when exposed to 60 μM despite its lower VDA activity (Figure S38-S43).

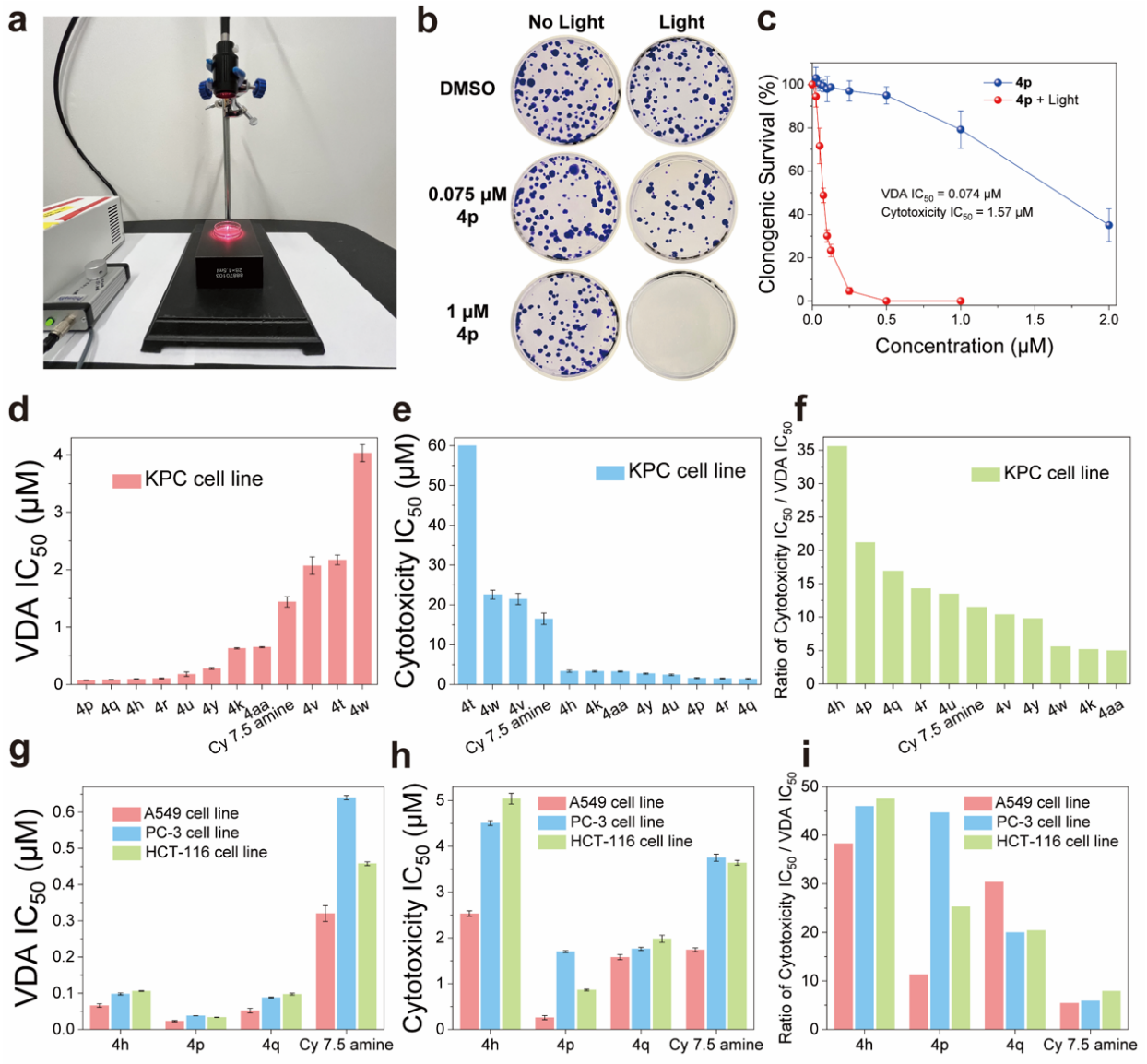

Figure 3. Survival and proliferative potential of cells assessment after treatment of MJH under 730 nm light (80 mW/cm^2, 10 min) and without light by clonogenic assay. a) Pictures of experimental set up to eradicate cancer cells. b) Representative pictures showing the growth of cell colonies in the controls (0.1% DMSO with or without light) and complete eradication of KPC cells when treated with 1 μM **4p** and light. c) Quantification of the number cells forming colonies was conducted to assess cell survival after treatment with **4p**. d) The lethal concentration of MJH

to kill 50% of KPC cells with light activation (VDA IC_{50}). e) The lethal concentration of MJH to kill 50% of KPC cells without light activation (cytotoxicity IC_{50}). f) The ratio of cytotoxicity IC_{50} / VDA IC_{50} for each MJH on KPC cells. g) The lethal concentration of **4h**, **4p**, **4q** and Cy7.5 amine to kill 50% of A549 cells, PC-3 cells and HCT-116 cells with light activation (VDA IC_{50}). h) The lethal concentration of **4h**, **4p**, **4q** and Cy7.5 amine to kill 50% of A549 cells, PC-3 cells and HCT-116 cells without light activation (cytotoxicity IC_{50}). i) The ratio of cytotoxicity IC_{50} / VDA IC_{50} for each molecule on A549 cells, PC-3 cells and HCT-116 cells. Error bars in the data represent the standard deviation and all results are normalized relative to the DMSO control, serving as a reference for comparison. The experimental design included three independent sample repetitions (n = 3).

Following this, we investigated the VDA efficiency of **4h**, **4p**, **4q** and Cy 7.5 amines on human cancer cell lines (lung cancer cells A549, prostate cancer cells PC-3 and colorectal cancer cells HCT-116),[26,61,62] as depicted in Figure 3g-i. The results were found to be consistent across these cell lines, comparable with the observations in KPC cells. As expected (Figure S44-S52), **4p** exhibited significantly higher VDA activity (VDA IC_{50} less than 40 nM, shown in Figure S44, S47 and S50) compared to other MJH among these three cell lines, while Cy 7.5 amine displayed the lowest activity. Remarkably, **4h** showed the highest phototherapy index, with more than a 7-fold improvement compared to Cy 7.5 amine in both A549 (7.8-fold) and PC-3 (7.1-fold) cell lines, along with a 6-fold improvement in HCT-116 cells (Figure 3i). Additionally, compound **4p** also

demonstrated a substantial improvement, up to 7.6-fold, albeit only 2.1-fold in A549 cells and 3.2-fold in HCT-116 cells. **4q** showed up to a 5.6-fold improvement in the A549 cell line, a 3.6-fold improvement in PC-3 cells, and a 2.9-fold improvement in HCT-116 cells in contrast with Cy 7.5 amine. These results underscore the wide applicability of **4h** in different cancer cell lines and highlight the significance of structural optimization, encouraging further exploration of the applications for NIR-activated MJH cancer treatment *in vivo*.

Conclusion

In summary, we have developed a practical method to construct cyclohexene-modified cyclic glutacondianil intermediates by a palladium-catalyzed dehalogenation reaction. This intermediate served as a platform for the formation of a variety of both symmetrical and nonsymmetrical Cy7 and Cy 7.5 MJH, provided in moderate to good yields with various functional substitutions on the heterocyclics. Additionally, we evaluated the photophysical properties of the substituted derivatives and demonstrated that side chains on heterocyclics showed minimal influence on the maximum absorption and emission wavelength, however, molar extinction coefficients and quantum yields were affected. Furthermore, we enhanced the high efficiency of VDA to permeabilize more cancer cell lines membranes, leading to cell death with low lethal concentrations, and enhanced the phototherapy index using MJH with dimethylaminoethyl and dimethylcarbamoyl substitutions. Mechanistic studies revealed a mechanical action of VDA to destroy the cells that was unaffected by high doses of ROS scavengers, highlighting their mode of

action that is distinct from PDT. This work provides a general synthetic approach and contributes to the synthetic methodologies for cyanine structural optimization based on structure-activity relationships, with encouraging results and prospects for cancer treatment.

Acknowledgments. Funding was provided by The Discovery Institute and The Welch Foundation (C-2017-20220330). The authors thank Prof. Angel A. Martí at Rice University for kindly sharing his laboratory to culture the cancer cells and thank Dr. D. K. James for editing the manuscript. The characterization equipment used in this project is from the Shared Equipment Authority (SEA) at Rice University.

Supporting Information. General information and procedures. Additional graphs and data. References. Copies of NMR spectra (PDF).

Competing Interests: Rice University owns intellectual property on the use of MJH for permeabilization of cell membranes. Nanorobotics Ltd. is the possible licensee of this technology from Rice University. J.M.T. is a stockholder in Nanorobotics Ltd., but not an officer, director, or employee. Conflicts are mitigated through regular disclosure to and compliance with the Rice University Office of Sponsored Programs and Research Compliance. The authors declare no other potential conflicts.

References

1. W. H. Clark, *Br. J. Cancer* **1991**, *64*, 631–644.
2. R. L. Siegel, K. D. Miller, N. S. Wagle, A. Jemal, *CA Cancer J. Clin.* **2023**, *73*, 17–48.
3. I. Soerjomataram, F. Bray, *Nat. Rev. Clin. Oncol.* **2021**, *18*, 663–672.
4. R. Sullivan, O. I. Alatise, B. O. Anderson, R. Audisio, P. Autier, A. Aggarwal, C. Balch, M. F. Brennan, A. Dare, A. D'Cruz, A. M. Eggermont, K. Fleming, S. M. Gueye, L. Hagander, C. A. Herrera, H. Holmer, A. M. Ilbawi, A. Jarnheimer, J.-F. Ji, T. P. Kingham, J. Liberman, A. J. Leather, J. G. Meara, S. Mukhopadhyay, S. S. Murthy, S. Omar, G. P. Parham, C. S. Pramesh, R. Riviello, D. Rodin, L. Santini, S. V. Shrikhande, M. Shrime, R. Thomas, A. T. Tsunoda, C. van de Velde, U. Veronesi, D. K. Vijaykumar, D. Watters, S. Wang, Y.-L. Wu, M. Zeiton, A. Purushotham, *Lancet Oncol.* **2015**, *16*, 1193–1224.
5. Y. Liu, L. Teng, B. Yin, H. Meng, X. Yin, S. Huan, G. Song, X.-B. Zhang, *Chem. Rev.* **2022**, *122*, 6850−6918.
6. M. Garland, J. J. Yim, M. Bogyo, *Cell Chem. Biol.* **2016**, *23*, 122-136.
7. S. Chen, S. Yu, Z. Du, X. Huang, M. He, S. Long, J. Liu, Y. Lan, D. Yang, H. Wang, S. Li, A. Chen, Y. Hao, Y. Su, C. Wang, S. Luo, *J. Med. Chem.* **2021**, *64*, 3381–3391.
8. H. Ma, Y. Lu, Z. Huang, S. Long, J. Cao, Z. Zhang, X. Zhou, C. Shi, W. Sun, J. Du, J. Fan, X Peng, *J. Am. Chem. Soc.* **2022**, *144*, 3477−3486.

9. H. Huang, S. Banerjee, K. Qiu, P. Zhang, O. Blacque, T. Malcomson, M. J. Paterson, G. J. Clarkson, M. Staniforth, V. G. Stavros, G. Gasser, H. Chao, P. J. Sadler, *Nat. Chem.* **2019**, *11*, 1041−1048.

10. B. M. Vickerman, E. M. Zywot, T. K. Tarrant, D. S. Lawrence, *Nat. Rev. Chem.* **2021**, *5*, 816–834.

11. J. S. D. Mieog, F. B. Achterberg, A. Zlitni, M. Hutteman, J. Burggraaf, R.-J. Swijnenburg, S. Gioux, A. L. Vahrmeijer, *Nat. Rev. Clin. Oncol.* **2022**, *19*, 9−22.

12. C. Shi, J. B. Wu, D. Pan, *J. Biomed. Opt.* **2016**, *21*, 050901.

13. T. C. Pham, V.-N. Nguyen, Y. Choi, S. Lee, J. Yoon, *Chem. Rev.* **2021**, *121*, 13454−13619.

14. K. Mitra, C. E. Lyons, M. C. T. Hartman, *Angew. Chem., Int. Ed.* **2018**, *57*, 10263−10267.

15. S. M. Usama, S. Thavornpradit, K. Burgess, *ACS Appl. Bio Mater.* **2018**, *1*, 1195−1205.

16. N. Lange, W. Szlasa, J. Saczko, A. Chwiłkowska, *Pharmaceutics* **2021**, *13*, 818.

17. X. Zhao, Q. Yao, S. Long, W. Chi, Y. Yang, D. Tan, X. Liu, H. Huang, W. Sun, J. Du, J. Fan, X. Peng, *J. Am. Chem. Soc.* **2021**, *143*, 12345−12354.

18. X. Zhou, C. Shi, S. Long, Q. Yao, H. Ma, K. Chen, J. Du, W. Sun, J. Fan, B. Liu, L. Wang, X. Chen, L. Sui, K. Yuan, X. Peng, *ACS Cent. Sci.* **2023**, *9*, 1679-1691.

19. H. S. Jung, P. Verwilst, A. Sharma, J. Shin, J. L. Sessler, J. S. Kim, *Chem. Soc. Rev.* **2018**, *47*, 2280−2297.

20. W. Bian, Y. Wang, Z. Pan, N. Chen, X. Li, W.-L. Wong, X. Liu, Y. He, K. Zhang, Y.-J. Lu, *ACS Appl. Nano Mater.* **2021**, *4*, 11353−11385.

21. A. St Lorenz, E. R. Buabeng, O. Taratula, O. Taratula, M. Henary, *J. Med. Chem.* **2021**, 64, 8798−8805.

22. G. Jo, E. J. Kim, H. Hyun, *Int. J. Mol. Sci.* **2023**, *24*, 862.

23. G. Kroemer, J. C. Reed, *Nat. Med.* **2000**, *6*, 513−519.

24. D. C. Wallace, *Nat. Rev. Cancer* **2012**, *12*, 685−698.

25. H. E. Barker, J. T. Paget, A. A. Khan, K. J. Harrington, *Nat. Rev. Cancer* **2015**, *15*, 409−425.

26. S. L. Luo, X. Tan, S. T. Fang, Y. Wang, T. Liu, X. Wang, Y. Yuan, H. Sun, Q. Qi, C. Shi, *Adv. Funct. Mater.* **2016**, *26*, 2826-2835.

27. X. S. Li, J. F. Lovell, J. Y. Yoon, X. Y. Chen, *Nat. Rev. Clin. Oncol*. **2020**, *17*, 657−674.

28. X. J. Zhao, H. J. Zhao, S. Wang, Z. W. Fan, Y. Ma, Y. M. Yin, W. Wang, R. M. Xi, M. Meng, *J. Am. Chem. Soc.* **2021**, *143*, 20828−20836.

29. H. Mustroph, A. Towns, *ChemPhysChem* **2018**, *19*, 1016–1023.

30. F.-F. Kong, X.-J. Tian, Y. Zhang, Y.-J. Yu, S.-H. Jing, Y. Zhang, G.-J. Tian, Y. Luo, J.-L. Yang, Z.-C. Dong, J. G. Hou, *Nat. Commun.* **2021**, *12*, 1280.

31. Y. Cui, A. Lauchner, A. Manjavacas, F. J. García de Abajo, N. J. Halas, P. Nordlander, *Nano Lett.* **2016**, *16*, 6390−6395.

32. T. C. Hung, B. Kiraly, J. H. Strik, A. A. Khajetoorians, D. Wegner, *Nano Lett.* **2021**, *21*, 5006–5012.

33. K. D. Chapkin, L. Bursi, G. J. Stec, A. Lauchner, N. J. Hogan, Y. Cui, P. Nordlander, N. J. Halas, *Proc. Natl. Acad. Sci.* **2018**, *115*, 9134−9139.

34. C. Ayala-Orozco, D. Galvez-Aranda, A. Corona, J. M. Seminario, R. Rangel, J. N. Myers, J. M. Tour, *Nat. Chem.* **2024**, *16*, 456–465.

35. C. Ayala-Orozco, G. Li, B. Li, V. Vardanyan, A. B. Kolomeisky, J. M. Tour, *Adv. Mater.* **2024**, *36*, 2309910.

36. C. Ayala-Orozco, V. Vardanyan, K. Lopez-Jaime, Z. Wang, J. Seminario, A. Kolomeisky, J. M. Tour, *ChemRxiv.* preprint, DOI: 10.26434/chemrxiv-2024-8cfcc.

37. L. Štacková, E. Muchová, M. Russo, P. Slavíček, P. Štacko, P. Klán, *J. Org. Chem.* **2020**, *85*, 9776−9790.

38. A. Mishra, R. K. Behera, P. K. Behera, B. K. Mishra, G. B. Behera, *Chem. Rev.* **2000**, *100*, 1973−2012.

39. W. Sun, S. Guo, C. Hu, J. Fan, X. Peng, *Chem. Rev.* **2016**, *116*, 7768−7817.

40. M. M. Leitão, D. de Melo-Diogo, C. G. Alves, R. Lima-Sousa, I. J. Correia, *Adv. Healthcare Mater.* **2020**, *9*, 1901665.

41. R. M. Exner, F. Cortezon-Tamarit, S. I. Pascu, *Angew. Chem., Int. Ed.* **2021**, *60*, 6230−6241.

42. S. M. Usama, C. Lin, K. Burgess, *Bioconjugate Chem.* **2018**, *29*, 3886−3895.

43. S. Pascal, A. Haefele, C. Monnereau, A. Charaf-Eddin, D. Jacquemin, B. Le Guennic, C. Andraud, O. Maury, *J. Phys. Chem. A* **2014**, *118*, 4038-4047.

44. S. G. König, R. Krämer, *Chem. – Eur. J.* **2017**, *23*, 9306−9312.

45. A. A. Fadda, R. E. El-Mekawy, *Dyes Pigm*. **2015**, *118*, 45-52.

46. A. A. Fadda, R. E. El-Mekawy, *Dyes Pigm*. **2013**, *99*, 512-519.

47. L. Štacková, P. Štacko, P. Klán, *J. Am. Chem. Soc.* **2019**, *141*, 7155-7162.

48. Z. Hao, L. Hu, X. Wang, Y. Liu, S. Mo, *Org. Lett.* **2023**, *25*, 1078–1082.

49. S. M. Usama, S. C. Marker, D. H. Li, D. R. Caldwell, M. Stroet, N. L. Patel, A. G. Tebo, S. Hernot, J. D. Kalen, M. Schnermann, *J. Am. Chem. Soc.* **2023**, *145*, 14647−14659.

50. M. Shamim, J. Dinh, C. Yang, S. Nomura, S. Kashiwagi, H. Kang, H. S. Choi, M. Henary, *ACS Pharmacol. Transl. Sci.* **2023**, *6*, 1192–1206.

51. Y. Ueno, J. Jose, A. Loudet, C. Pérez-Bolívar, P. Anzenbacher, K. Burgess, *J. Am. Chem. Soc.* **2011**, *133*, 51-55.

52. D. S. Pisoni, L. Todeschini, A. C. A. Borges, C. L. Petzhold, F. S. Rodembusch, L. F. Campo, *J. Org. Chem.* **2014**, *79*, 5511−5520.

53. N. Wolf, L. Kersting, C. Herok, C. Mihm, J. Seibel, *J. Org. Chem.* **2020**, *85*, 9751−9760.

54. B. E. Schaafsma, J. S. D. Mieog, M. Hutteman, J. R. van der Vorst, P. J. K. Kuppen, C. W. G. M. Löwik, J. V. Frangioni, C. J. H. van de Velde, A. L. Vahrmeijer, *J. Surg. Oncol.* **2011**, *104*, 323−332.

55. C. Ayala-Orozco, D. Liu, Y. Li, L. B. Alemany, R. Pal, S. Krishnan, J. M. Tour, *ACS Appl. Mater. Interfaces* **2020**, *12*, 410−417.

56. J. W. Lee, C. A. Komar, F. Bengsch, K. Graham, G. L. Beatty, *Curr. Protoc. Pharmacol.* **2016**, DOI: 10.1002/cpph.2.

57. M. Hirth, Y. Xie, C. Höper, A. Prats, T. Hackert, M. P. Ebert, R. Kuner, *Cells* **2022**, *11*, 2634.

58. S. R. Hingorani, L. Wang, A. S. Multani, C. Combs, T. B. Deramaudt, R. H. Hruban, A. K. Rustgi, S. Chang, D. A. Tuveson, *Cancer Cell* **2005**, *7*, 469-483.

59. J. L. Beckham, T. S. Bradford, C. Ayala-Orozco, A. L. Santos, D. Arnold, A. R. van Venrooy, V. García-López, R. Pal, J. M. Tour, *Adv. Mater.* **2024**, *36*, 2306669.

60. N. A. P. Franken, H. M. Rodermond, J. Stap, J. Haveman, C. van Bree, *Nat. Protoc.* **2006**, *1*, 2315–2319.

61. J. B. Wu, T.-P. Lin, J. D. Gallagher, S. Kushal, L. W. K. Chung, H. E. Zhau, B. Z. Olenyuk, J. C. Shih, *J. Am. Chem. Soc.* **2015**, *137*, 2366−2374.

62. P. Xiao, W. Xie, J. Zhang, Q. Wu, Z. Shen, C. Guo, Y. Wu, F. Wang, B. Z. Tang, D. Wang, *J. Am. Chem. Soc*. **2023**, *145*, 334−344.

Table of Contents Graphic